Emmanuel Motheau[1]
CERFACS - CFD Team
42 av. Gaspard Coriolis,
31057 Toulouse, France
e-mail: emmanuel.motheau@cerfacs.fr

Franck Nicoud
CNRS UMR 5149,
University Montpellier II,
34095 Montpellier, France
e-mail: franck.nicoud@univ-montp2.fr

Thierry Poinsot
CNRS - Institut de Mécanique des Fluides,
1 Allée du Professeur Camille Soula,
31000 Toulouse, France
e-mail: thierry.poinsot@cerfacs.fr

Using Boundary Conditions to Account for Mean Flow Effects in a Zero Mach Number Acoustic Solver

The present study is devoted to the modeling of mean flow effects while computing thermoacoustic modes under the zero Mach number assumption. It is first recalled that the acoustic impedance modeling of a compressor or a turbine must be prescribed under an energetical form instead of the classical acoustic variables. Then we demonstrate the feasibility to take into account the coupling between acoustic and entropy waves in a zero Mach number framework to capture a family of low frequency entropic modes. The proposed approach relies on a new delayed entropy coupled boundary condition (DECBC) and proves able to capture a family of low frequency entropic mode even though no mean flow term is included in the fluctuating pressure equation. [DOI: 10.1115/1.4007198]

1 Introduction

Lean premixed combustor systems in aero-engines are promising devices to meet the future NO_x emission reduction requirements. However, they are also more prone to combustion instabilities compared to classical combustors [1]. These oscillations of the flow may lead to many undesirable effects, such as large-amplitude structural vibrations, flame flashback or blowoff, or an abnormally high temperature of the wall of the combustor. In the best case, the consequences would be a simple loss of performance or a premature fatigue of materials. In the worst case, a spectacular destruction of the system can occur. Consequently, there is a need to better understand combustion instabilities and to be able to predict them at the design level.

Several methods have been developed to study these instabilities, such as low-order methods [2,3] which solve only the unidimensional acoustic problems, or at the opposite the large eddy simulation (LES) which solves numerically the complete flow thanks to the reactive Navier-Stokes equations. As an intermediate, the problem complexity can be reduced by the derivation of the linearized Euler equations (LEE) which neglect viscous effects, or by the derivation of the Helmholtz equation when neglecting the mean flow motion. Although this last method may be a crude simplification of the problem, this approach combined with LES proved useful to better understand the structure and nature of the instabilities observed in academic or industrial burners [4].

Although it is tempting to restrict the study of the behavior of thermo-acoustic instabilities to only the combustion chamber, it is however important to take into account the proper acoustic environment of the gas turbine, as for example the presence of a compressor or a high pressure distributor. Since it is difficult to simulate the whole configuration, a possibility is to reduce the computational domain to only the flame tube where the mean Mach number is approximately zero $(M = 0)$ while the compressor and the turbine are modeled by prescribing appropriate complex valued impedances at the boundaries.

At least two difficulties arise when using a Helmholtz solver (thus assuming $M = 0$) for the combustion chamber and boundary impedances to represent the upstream/downstream environment:

- In order to match the zero Mach number assumption used to formulate the thermo-acoustic problem, the impedance should be defined in theory in a section of the combustion chamber where the Mach number is very small. In practice, the location of the outlet section is often imposed by geometrical considerations and the effective Mach number at the boundary is not necessarily very small.
- Three modes of fluctuations can perturb a steady baseline flow [5]: acoustic perturbations propagates at the speed of sound augmented by the local mean velocity while vortical and entropy perturbations are simply convected by the mean flow. As a consequence, the zero Mach number assumption necessarily neglect the convection of entropy or vorticity spots to the downstream. As shown by many authors [6–9], entropy inhomogeneities generate acoustic waves when accelerated in a mean flow pressure gradient, which is the case when the combustor opens onto a high pressure distributor. Acoustic waves transmitted through the distributor generate *indirect combustion noise*, while acoustic waves traveling back to the flame may generate a low frequency resonant mode called *rumble* [10,11].

It has been demonstrated in a previous study [12] that the zero Mach number assumption for the mean flow can lead to significant errors both in the prediction of the frequency and the growth rate of the thermo-acoustic mode, suggesting that the two points described above are of major importance. Since accounting for the nonzero Mach number terms in the equations leads to a drastic increase of the problem complexity [13], the aim of this paper is to investigate an alternative approach where the thermo-acoustic problem in the domain is still solved under the zero Mach number assumption and the coupling with the convective quantities is modeled through an appropriate downstream boundary condition.

The basic equations are recalled in Sec. 2, while in Sec. 3 the proper way to couple a Helmholtz solver with an analytical and/or numerical tool for the computation of the upstream/downstream boundary impedance is discussed. In Sec. 4 we demonstrate the feasibility to take into account the coupling between acoustic and entropy waves in a zero Mach number framework and to capture a family of low frequency entropic modes. The analysis focuses on the configuration of a simple tube containing a flame and where a shocked nozzle is located downstream.

2 Mathematical Formalism

This study is conducted in the frequency domain, i.e., $g'(x,t) = \Re\{\hat{g}(x)e^{-j\omega t}\}$ for any fluctuating quantity; it also

[1]Corresponding author.

Contributed by the International Gas Turbine Institute (IGTI) of ASME for publication in the JOURNAL OF ENGINEERING FOR GAS TURBINES AND POWER. Manuscript received June 25, 2012; final manuscript received July 13, 2012; published online September 24, 2012. Editor: Dilip R. Ballal.

focuses on unidimensional configurations so that only purely longitudinal acoustic and entropy convection effects are present. Consequently, vorticity perturbations and their interactions with the acoustics are neglected in the remainder of the whole study.

2.1 Linearized Euler Equations for the Eigenvalue Problem. For a homogeneous reacting mixture with constant heat capacities C_p and C_v, the linearized harmonic form of conservation equations for mass, momentum, and energy in a quasi-1D domain of cross section area $S(x)$ read, respectively,

$$\hat{u}\frac{\partial \rho_0}{\partial x}+\rho_0\frac{\partial \hat{u}}{\partial x}+u_0\frac{\partial \hat{\rho}}{\partial x}+\hat{\rho}\frac{\partial u_0}{\partial x}+\frac{\rho_0\hat{u}+\hat{\rho}u_0}{S}\frac{\partial S}{\partial x}=j\omega\hat{\rho} \quad (1)$$

$$\frac{1}{\rho_0}\frac{\partial \hat{p}}{\partial x}+\hat{u}\frac{\partial u_0}{\partial x}+u_0\frac{\partial \hat{u}}{\partial x}+\frac{u_0\hat{\rho}}{\rho_0}\frac{\partial u_0}{\partial x}=j\omega\hat{u} \quad (2)$$

$$\hat{u}\frac{\partial s_0}{\partial x}+u_0\frac{\partial \hat{s}}{\partial x}+\frac{rq_0}{p_0^2}\hat{p}-\frac{r}{p_0}\hat{q}=j\omega\hat{s} \quad (3)$$

with the linearized state equation and entropy expression,

$$\frac{\hat{p}}{p_0}-\frac{\hat{\rho}}{\rho_0}-\frac{\hat{T}}{T_0}=0 \quad \text{and} \quad \frac{\hat{s}}{C_v}=\frac{\hat{p}}{p_0}-\gamma\frac{\hat{\rho}}{\rho_0} \quad (4)$$

Assuming that the unsteady heat release amplitude $\hat{q}$ is modeled as a linear operator, i.e., $\hat{q}=q_{\hat{\rho}}\hat{\rho}+q_{\hat{u}}\hat{u}+q_{\hat{s}}\hat{s}$, Eqs. (1)–(3) define an eigenvalue problem $\mathcal{M}\mathcal{W}=j\omega\mathcal{W}$, where $\mathcal{M}$ is:

$$\begin{bmatrix} \frac{\partial u_0}{\partial x}+u_0\frac{\partial}{\partial x}+\frac{u_0}{S}\frac{\partial S}{\partial x} & \frac{\partial \rho_0}{\partial x}+\rho_0\frac{\partial}{\partial x}+\frac{\rho_0}{S}\frac{\partial S}{\partial x} & 0 \\ \frac{1}{\rho_0}\frac{\partial c_0^2}{\partial x}+\frac{u_0}{\rho_0}\frac{\partial u_0}{\partial x}+\frac{c_0^2}{\rho_0}\frac{\partial}{\partial x} & \frac{\partial u_0}{\partial x}+u_0\frac{\partial}{\partial x} & \mathcal{T}\left(\frac{1}{p_0}\frac{\partial p_0}{\partial x}+\frac{\partial}{\partial x}\right) \\ \frac{\gamma r q_0}{\rho_0 p_0}-\frac{r}{p_0}q_{\hat{\rho}} & \frac{\partial s_0}{\partial x}-\frac{r}{p_0}q_{\hat{u}} & u_0\frac{\partial}{\partial x}+\frac{\mathcal{T}}{T_0}\frac{q_0}{p_0}-\frac{r}{p_0}q_{\hat{s}} \end{bmatrix} \quad (5)$$

and $(\omega,\mathcal{W})$ the eigenpair, the eigenvector being $\mathcal{W}=(\hat{\rho},\hat{u},\hat{s})^T$, S the varying area section, and $\mathcal{T}=(\gamma-1)T_0$.

2.2 Plane Waves in an Homogeneous Media. In the case of a 1D domain with homogeneous baseline flow, the following expressions can be obtained [14] for the complex amplitudes,

$$\hat{p}(x)=A^+e^{jk^+x}+A^-e^{-jk^-x} \quad (6)$$

$$\hat{u}(x)=\frac{1}{\rho_0 c_0}[A^+e^{jk^+x}-A^-e^{-jk^-x}] \quad (7)$$

$$\hat{s}(x)=\sigma e^{jk_s x} \quad (8)$$

with

$$k^+=\frac{\omega}{c_0+u_0}=\frac{k}{1+M} \quad k^-=\frac{\omega}{c_0-u_0}=\frac{k}{1-M} \quad (9)$$

$$k_s=\frac{k}{M} \quad (10)$$

where A^+ and A^- are the amplitudes of the forward and backward propagating acoustic waves, respectively, σ is the amplitude of the forward propagating entropic wave, $k=\omega/c_0$ is the acoustic wave number, and M is the Mach number. It should be noted that Eq. (8) represents an idealistic situation where the spatial diffusion of entropy spots is neglected. Although this situation is not supported by previous studies [15], it is judged appropriate for this proof of concept study.

Injecting the above expression of entropy into Eq. (4) leads to

$$\hat{\rho}=\frac{\hat{p}}{c_0^2}-\frac{\rho_0\sigma}{C_p}e^{jk_s x} \quad \text{and} \quad \frac{\hat{T}}{T_0}=\frac{\gamma-1}{\rho_0 c_0^2}\hat{p}+\frac{\sigma}{C_p}e^{jk_s x} \quad (11)$$

Equations (6), (7), and (11) describe the harmonic small amplitude perturbations in the domain. Relations between complex valued amplitudes A^+, A^-, and σ are prescribed by boundary conditions and jump relations through the interfaces.

3 Influence of the Boundary Impedance on Thermo-Acoustic Eigenfrequencies

When studying the acoustic behavior of a combustor by computing the eigenmodes thanks to a Helmholtz solver, appropriate boundary conditions must be used in order to represent the acoustic environment. Upstream/downstream impedances can be deduced from transfer functions describing the response of acoustic elements to acoustic or entropic perturbations, either analytically under the compact hypothesis [16] or numerically by solving the LEEs [17]. The impedance should be defined in a section of the combustion chamber where the Mach number is *very small*, consistently with the zero Mach number assumption which is valid when $M \ll L_f/L_a$, where L_f is the thickness of the reaction zone and L_a is the typical acoustic wavelength. Since this is not always the case in practice, there is a need to quantify the errors inherent to this practice when the outlet/inlet Mach number is not *very small*.

The configuration considered is shown in Fig. 1(*a*). It consists of two connected tubes of section S_1 and S_2. The subscripts 1 and 2 refer to parameters in the left and right tube, respectively. Only isentropic fluctuations are considered (the inlet boundary condition is $s'=0$ and there is no entropy source within the flow domain).

The eigenmodes of this simple configuration are computed by four different methods to assess the errors made when the boundary Mach number increases and deduce the proper way to prescribe boundary impedance.

3.1 Method A0: Numerical Results From the LEEs. The LEEs presented in Sec. 2.1 are solved numerically so as to provide a reference solution accounting for mean flow effects and the complete geometry [12].

3.2 Method A1: Global Acoustic Model. The forward and backward waves traveling in both tubes lead to four unknown A_1^+, A_1^-, A_2^+, and A_2^-. These waves are solutions of an homogeneous linear system of equations obtained by requiring that the boundary

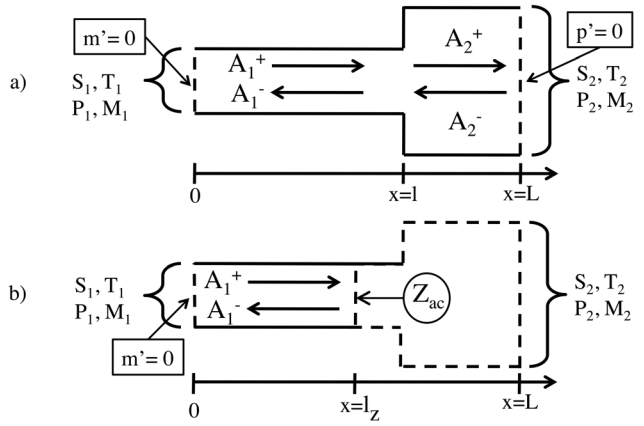

Fig. 1 Configuration *A* investigated in Sec. 3. (*a*) The complete geometry is computed. (*b*) Only a part of the tube 1 is computed while the rest of the domain is modeled through downstream impedance.

conditions and jump relations are fulfilled. The two boundary conditions form a first set of relations between wave amplitudes. A constant mass-flow rate $m'_1 = 0$ is imposed at the inlet $x = 0$ of the domain, while the outlet at $x = L$ is modeled by an acoustic open-end, so that $p'_2 = 0$. Introducing the plane wave decomposition of pressure and velocity fluctuations leads to

$$A_1^+(1+M_1) - A_1^-(1-M_1) = 0 \quad \text{at } x = 0 \tag{12}$$

$$A_2^+ e^{jk_2^+ L} + A_2^- e^{-jk_2^- L} = 0 \quad \text{at } x = L \tag{13}$$

As explained in [14] the jump relations for the section change located at $x = l$ can be expressed by integrating over an infinitesimal control volume the conservation of mass (Eq. (1)) where the time averaged mass flux term has been subtracted, and energy (Eq. (3)) as long as the specific stagnation enthalpy within the volume remains invariant. The following set of equations is then obtained:

$$\left[(1+M_1)A_1^+ e^{jk_1^+ l} - (1-M_1)A_1^- e^{-jk_1^- l}\right]\frac{S_1}{c_1} = \left[[(1+M_2)A_2^+ e^{jk_2^+ l} - (1-M_2)A_2^- e^{-jk_2^- l}\right]\frac{S_2}{c_2} \tag{14}$$

$$\left[(1+M_1)A_1^+ e^{jk_1^+ l} + (1-M_1)A_1^- e^{-jk_1^- l}\right]\frac{1}{\rho_1} = \left[[(1+M_2)A_2^+ e^{jk_2^+ l} + (1-M_2)A_2^- e^{-jk_2^- l}\right]\frac{1}{\rho_2} \tag{15}$$

One obtains the algebraic system $\mathcal{M}\mathcal{W} = 0$, where $\mathcal{M}$ is defined as

$$\begin{bmatrix} M_1^+ & -M_1^- & 0 & 0 \\ 0 & 0 & e^{jk_2^+ L} & e^{-jk_2^- L} \\ \frac{S_1}{c_1}M_1^+ e^{jk_1^+ l} & -\frac{S_1}{c_1}M_1^- e^{-jk_1^- l} & -\frac{S_2}{c_2}M_2^+ e^{jk_2^+ l} & \frac{S_2}{c_2}M_2^- e^{-jk_2^- l} \\ M_1^+\frac{\rho_2}{\rho_1}e^{jk_1^+ l} & M_1^-\frac{\rho_2}{\rho_1}e^{-jk_1^- l} & -M_2^+ e^{jk_2^+ l} & -M_2^- e^{-jk_2^- l} \end{bmatrix} \tag{16}$$

where $M_1^+ = (1+M_1)$, $M_1^- = (1-M_1)$, $M_2^+ = (1+M_2)$, $M_2^- = (1-M_2)$, and $\mathcal{W} = (A_1^+, A_1^-, A_2^+, A_2^-)^T$. The dispersion relation is then obtained by requiring the matrix $\mathcal{M}$ to be singular, producing the solution of the acoustical problem.

3.3 Method A2: Modeling of the Section Change by an Impedance. As shown in Fig. 1(*b*) the computational domain is reduced to the region between the inlet $x = 0$ where the boundary condition is still $m'_1 = 0$ and $x = l_z < l$ where the impedance Z_{ac} is imposed. The algebraic system described at Eq. (16) reduces to

$$\begin{bmatrix} (1+M_1) & -(1-M_1) \\ (1-Z_{ac})e^{jk_1^+ l_Z} & (1+Z_{ac})e^{-jk_1^- l_Z} \end{bmatrix}\begin{bmatrix} A_1^+ \\ A_1^- \end{bmatrix} = 0 \tag{17}$$

The impedance Z_{ac} is defined by

$$Z_{ac} = \frac{1+R_{ac}}{1-R_{ac}} \tag{18}$$

where $R_{ac} = A_1^-/A_1^+$ is the coefficient of reflection defined as the ratio between the reflected and the incident wave. The transfer function of the modeled part of the domain $(l_z < x < L)$ can be found by setting A_1^+ to unity so as to express A_1^-. After cumbersome but straightforward algebra, Eq. (16) leads to

$$R_{ac} = e^{\frac{2jk_1(l-l_Z)}{1-M_1^2}}\left(\frac{1+M_1}{1-M_1}\right)\left(\frac{\mathcal{A}+\mathcal{B}}{\mathcal{A}-\mathcal{B}}\right) \tag{19}$$

with

$$\mathcal{A} = \frac{S_1}{c_1}\left[(1-M_2)e^{\frac{2jk_2(L-l_Z)}{1-M_2^2}} - (1+M_2)e^{\frac{2jk_2(l-l_Z)}{1-M_2^2}}\right] \tag{20}$$

$$\mathcal{B} = \frac{S_2}{c_2}\frac{\rho_2}{\rho_1}\left[(1-M_2)e^{\frac{2jk_2(L-l_Z)}{1-M_2^2}} + (1+M_2)e^{\frac{2jk_2(l-l_Z)}{1-M_2^2}}\right] \tag{21}$$

3.4 Method A3: Zero Mach Number Domain. Method A3 is similar to method A2 as described above. The only difference is the use in the computational domain of a wave number k derived under the zero Mach number assumption instead of $k^\pm$ and M_1 is set to zero in Eq. (17). The relation $A_1^+ - A_1^- = 0$ is now imposed at $x = 0$. Moreover, the expression of the impedance Z_{ac} and the reflection coefficient R_{ac} remains unchanged. Thus, Eq. (17) becomes

$$\begin{bmatrix} 1 & -1 \\ (1-Z_{ac})e^{jk_1 l_Z} & (1+Z_{ac})e^{-jk_1 l_Z} \end{bmatrix}\begin{bmatrix} A_1^+ \\ A_1^- \end{bmatrix} = 0 \tag{22}$$

3.5 Results. Thermodynamic and geometrical parameters used for the computation of eigenmodes are presented in Table 1. The temperature T_1 and pressure P_1 are imposed to the computation, while these parameters with the subscript 2 are deduced from the steady mean flow equations.

Results are presented in Table 2. As expected, comparisons between method **A0** and the global acoustical model (method **A1**) give very satisfying results. Real and imaginary parts of the frequency of the first eigenmode are both very close when computed at different inlet Mach number M_1. The small but existing difference can be explained by the fact that the length of the section change between S_1 and S_2 is not zero in the LEE solver but close to $x = 0.5$ mm.

Comparisons between methods **A1** and **A2** prove that truncating the computational domain while modeling the unresolved part

Table 1 Thermodynamic and geometrical parameters used in the configuration

S_1	S_2	T_1	P_1	γ	r	L	l	l_Z
0.05 m^2	0.1 m^2	300 K	101325 Pa	1.4	287 SI	1 m	0.99 m	0.98 m

Table 2 Results for the first eigenmode with methods A0, A1, A2, A3 with R_{ac} and A3* with R_e, for different inlet Mach number M_1

M_1	0.0005	0.1
A0	$87.154 - 0.007i$	$86.37 - 1.360i$
A1	$87.233 - 0.007i$	$86.367 - 1.364i$
A2	$87.233 - 0.007i$	$86.367 - 1.364i$
A3 (R_{ac})	$87.233 + 0.0208i$	$87.226 + 4.194i$
A3* (R_e)	$87.233 - 0.0007i$	$87.226 - 1.377i$

through an impedance gives exactly the same results. Based on this observation, the influence of the zero Mach number assumption can be isolated. Computations with method **A3** are chosen so as to represent the extreme case where 98% of the domain is solved with a zero mean flow. It is obvious that in such configuration the real part of the frequency f_M computed with Mach number effects will be very close to the one (f_0) computed at very low Mach number. As shown in [12] a relation between frequencies can be found, so that $f_M \approx (1 - M^2)f_0$. Verification of this relation with results of Table 2 is rather straightforward. The imaginary parts computed from method **A3** suggest that energy is entering into the domain while the Mach number increases. This observation is in contradiction with results from the reference methods which show that the first mode is always damped ($f_i < 0$). The solid line in Fig. 2 shows the modulus evolution of the reflection coefficient for different inlet Mach numbers M_1 (note that $|R_{ac}|$ does not depend on the frequency according to Eq. (19)). It is obvious that nonphysical energy growth is generated because the ratio between the reflected wave and the incoming wave is superior to unity. As explained in [18], $|R_{ac}|$ can exceed unity at a critical Strouhal number where vortical energy is generated downstream of an abrupt change in the geometry of a pipe. As vorticity is neglected in the present study, another explanation must be provided.

3.6 Boundary Conditions: From a Nonstationary Flow Formalism to a Zero Mach Number Formulation. As shown by many authors [6,19], the classical derivation of acoustic disturbances must be reformulated to take into account the convection of mechanical work by the mean flow. The starting point is to find an appropriate expression of the energy flux through a boundary [9], using fluctuating stagnation enthalpy J' and mass flow rate m' as state variables. A mathematical proof of the accuracy of such a choice for generalized acoustic field may be found in [20].

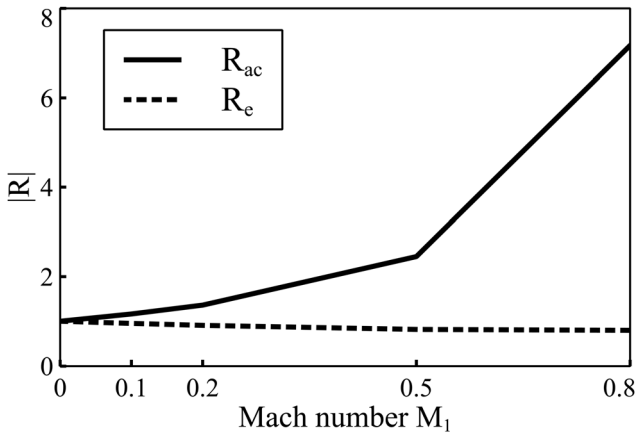

Fig. 2 Modulus of the reflection coefficient as a function of inlet Mach number M_1. Solid line: Acoustical formulation. Dashed line: Energetical formulation.

Defining first the total enthalpy $J = C_pT + \frac{1}{2}\mathbf{u}^2$ and the mass flow rate $m = \rho\mathbf{u}$, the linearized isentropic fluctuating part of these variables reads

$$\hat{J} = \frac{\hat{p}}{\rho_0} + u_0\hat{u} \tag{23}$$

$$\hat{m} = \rho_0\hat{u} + u_0\hat{\rho} \quad \text{with} \quad \hat{\rho} = \frac{\hat{p}}{c_0^2} \tag{24}$$

Reformulation of Eqs. (23) and (24) with the plane wave expansion of the pressure (Eq. (6)) and velocity (Eq. (7)) leads to

$$\hat{J} = J^+ + J^- = \frac{A^+(1+M)e^{jk^+x}}{\rho_0} + \frac{A^-(1-M)e^{-jk^-x}}{\rho_0} \tag{25}$$

$$\hat{m} = m^+ + m^- = \frac{A^+(1+M)e^{jk^+x}}{c_0} - \frac{A^-(1-M)e^{-jk^-x}}{c_0} \tag{26}$$

The methodology to express in a general manner a boundary condition in the zero-Mach number framework is described as follows:

1. The boundary condition must be prescribed first with energetic variables without neglecting the mean flow, defining then a functional $f(\hat{J}, \hat{m}, \hat{s}) = 0$ linking the fluctuating variables $\hat{J}$ (total enthalpy), $\hat{m}$ (mass), and $\hat{s}$ (entropy). Expanded each fluctuating quantity into waves (see Eqs. (25), (26), and (8)), the boundary condition is written under the form,

$$g(J^+, J^-, m^+, m^-, \sigma) = 0 \tag{27}$$

2. When the computational domain is represented under the zero Mach number assumption, the functional $f(\hat{J}, \hat{m}, \hat{s}) = 0$ describing the boundary condition remains unchanged. However, the energetic variables $\hat{J}$, $\hat{m}$, and $\hat{s}$ must be then expressed at the limit when $M \to 0$. It comes

$$\hat{J} = \frac{\hat{p}}{\rho_0} \quad \hat{m} = \rho_0\hat{u} \quad \hat{s} = 0 \tag{28}$$

As far as the waves are concerned, Eqs. (25) and (26) become when $M \to 0$,

$$\begin{aligned} J^+ &= \frac{A^+e^{jkx}}{\rho_0}, \quad J^- = \frac{A^-e^{-jkx}}{\rho_0} \\ m^+ &= \frac{A^+e^{jkx}}{c_0}, \quad m^- = -\frac{A^-e^{-jkx}}{c_0} \end{aligned} \tag{29}$$

Thus, the functional relationship representing the boundary condition under the zero Mach number assumption becomes

$$g\left(\frac{A^+e^{jkx}}{\rho_0}, \frac{A^-e^{-jkx}}{\rho_0}, \frac{A^+e^{jkx}}{c_0}, -\frac{A^-e^{-jkx}}{c_0}, 0\right) = 0 \tag{30}$$

As an illustration, this methodology is now applied to the boundary conditions used in the present study:

Boundary Condition. $\hat{m} = 0$: For that case, the functional $f(\hat{J}, \hat{m}, \hat{s}) = 0$ is $\hat{m} = 0$. Reformulating this condition using waves J^+, J^-, m^+, m^- and introducing the limiting behavior when $M \to 0$ leads to

$$m^+ + m^- = 0 \tag{31}$$

$$\frac{A^+}{c_0} - \frac{A^-}{c_0} = 0 \tag{32}$$

At the boundary where $\hat{m} = 0$, the input energetical reflection coefficient R_e defined as the ratio between the reflected wave A^+

and the incident wave A^- becomes $R_e = 1$, which may be viewed as $R_e = R_{ac}$ where R_{ac} is the classical acoustical reflection coefficient, which is $+1$ for $\hat{u} = 0$. This result explains in a proper way the validity of $\hat{u}_1 = 0$ as a choice for the input boundary condition in method A3.

Boundary Condition. $\hat{p} = 0$: Combining Eqs. (23) and (24) with $\hat{p} = 0$ leads to the functional $f(\hat{J}, \hat{m}, \hat{s}) = 0$,

$$\hat{J} - \frac{u_0}{\rho_0}\hat{m} = 0 \tag{33}$$

Reformulating with waves and using the limiting behaviors Eq. (29) leads to

$$(J^+ + J^-) = \frac{u_0}{\rho_0}(m^+ + m^-) \tag{34}$$

$$A^+(1 - M) = -A^-(1 + M) \tag{35}$$

At the boundary where $\hat{p} = 0$, the energetical reflection coefficient R_e defined as the ratio between the reflected wave A^- and the incident wave A^+ becomes $R_e = -((1 - M)/(1 + M))$ which may be viewed as

$$R_e = \left(\frac{1 - M}{1 + M}\right) R_{ac} \tag{36}$$

where R_{ac} is the classical acoustical reflection coefficient, which is -1 for $\hat{p} = 0$. This latter result can be directly applied to Eq. (19). Injection of R_e into 18 leads to an energetical impedance which takes the form of a ratio between stagnation enthalpy and mass fluctuations,

$$Z_e = \frac{\rho_1}{c_1}\frac{\hat{J}}{\hat{m}} \tag{37}$$

The dashed line in Fig. 2 shows the evolution of $|R_e|$ as a function of inlet Mach number M_1. As discussed in [18], the reflection coefficient R_e defined with the acoustical energy formulation is always equal or inferior to unity, suggesting that the continuity of the energy at the control surface is respected.

Computation of eigenmodes are now performed with R_e instead of R_{ac}. Results are presented in Table 2 under the column **A3***. Eigenfrequencies computed with a reflection coefficient based on the acoustic energy description are very close to the ones computed with the reference methods (**A0** and **A1**). As the real part of the frequency remains unchanged whatever the choice of the formulation of R, it suggests that the absorption of acoustical energy is included only through the formulation of the impedance. The small discrepancies between the reference solution and method **A3** with R_{ac} are related to the length of the domain where the Mach number is neglected. Actually, it can be shown that the frequency tends to the reference solution when l_Z approaches $x = 0$. Such results demonstrate that the impedance must be prescribed under an energetical form in order to obtain an appropriate representation of the whole configuration in the case where the domain is computed under the zero Mach number assumption.

4 Accounting for Entropy Convection in a Zero Mach Mean Flow

The acoustic waves generation when entropy inhomogeneities are accelerated in a nonuniform flow is a well-known phenomenon that has been extensively studied over the past decades. Early analytical investigations deal with the development of the jet noise theory, extending the work of Lighthill to nonuniform density flows [6–8]. However, these analytical solutions were limited to low Mach number flows and focused on the derivation of a formulation for the far-field sound radiation into free space by

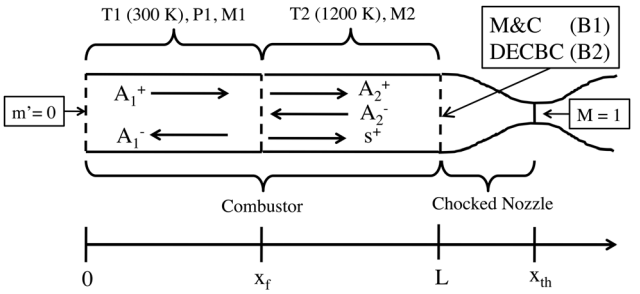

Fig. 3 Configuration *B* investigated in Sec. 4

inhomogeneities swept out of the nozzle orifice. In a different way, Marble and Candel [16] proposed a one-dimensional theory based on the compact assumption (the nozzle dimensions are small in comparison with the shortest wave length that appears in the flow field). The nozzle may be viewed as a duct discontinuity and simple relations between upstream/downstream acoustic and entropy waves can be written. Validation of such a theory has been provided recently [21] by comparisons with experiments.

The effect on thermoacoustic instabilities of the presence of a nozzle at the combustor exit is not obvious. As reviewed by [22] some authors found no difference on the thermoacoustic modes of their combustor whatever the type of exit used, while other authors [23] reported that a strong low-frequency instability occurred when the open exit was replaced by a chocked nozzle. As explained by [22], the behavior of such an instability depends to the first order on the geometry. The spatial dispersion of entropy fluctuations by the combustor aerodynamics [15] or the constructive/destructive phase dependency [10] play an important role for the establishment of a coupling between acoustic and entropy modes.

The configuration depicted in Fig. 3 has been chosen in order to exhibit the presence of an entropy mode among acoustic modes. A flame is located at $x = x_f$, which constitutes an interface between cold gas and hot gas. A chocked nozzle is located at $x = L$ while the sonic throat where the Mach number reaches unity is located at $x = x_{\text{th}}$. A similar methodology to the previous section is employed by comparing three methods.

4.1 Method B0: Numerical Reference Method.

Method **B0** is strictly the same as method **A0** presented above in Sec.2.1 [12]. Both the combustor and the nozzle are computed. The thickness of the flame is 0.005 m.

4.2 Method B1: Global Thermoacoustic Model.

Five equations are required to express the global thermoacoustic model. The flame is considered infinitely small, allowing the integration of conservation equations (1)–(3) over the discontinuity. At a first approximation and in the case where the two connected ducts share the same cross section S, this leads to the following set of jump relations [2]:

$$\rho_1\hat{u}_1 + u_1\hat{\rho}_1 = \rho_2\hat{u}_2 + u_2\hat{\rho}_2 \tag{38}$$

$$\hat{p}_1 + 2\rho_1 u_1\hat{u}_1 + u_1^2\hat{\rho}_1 = \hat{p}_2 + 2\rho_2 u_2\hat{u}_2 + u_2^2\hat{\rho}_2 \tag{39}$$

$$C_pT_{01}(\rho_1\hat{u}_1 + \hat{\rho}_1u_1) + \rho_1u_1\left(C_p\hat{T}_1 + u_1\hat{u}_1\right) = C_pT_{02}(\rho_2\hat{u}_2 + \hat{\rho}_2u_2) + \rho_2u_2\left(C_p\hat{T}_2 + u_2\hat{u}_2\right) \tag{40}$$

where Eq. (3) has been reformulated to express the total energy under a conservative form and the total unsteady heat release has been neglected. The mean stagnation temperature is $T_{0i} = T_i + \frac{1}{2}u_{0i}^2/C_p$ where the subscript $i = 1, 2$ refers to cold and hot gas, respectively.

The inlet and outlet boundary conditions form the last two equations that are closing the problem. At $x = 0$, the boundary condition imposed is $\hat{m}_1 = 0$. As recalled by [21], the compact relation that models the supersonic chocked nozzle at $x = L$ reads

$$\frac{\hat{u}_2(L)}{c_2} - \left(\frac{\gamma-1}{2}\right)M_2\frac{\hat{p}_2(L)}{\gamma P_2} - \frac{1}{2}M_2\frac{\hat{s}_2(L)}{C_p} = 0 \tag{41}$$

Using the usual plane wave expansions and Eqs. (38)–(41), the eigenfrequencies of the problem are computed by solving $\det(\mathcal{M}) = 0$, where $\mathcal{M}$ is the matrix,

$$\begin{bmatrix} M_1^+ e^{jk_1^+ x_f} & -M_1^- e^{-jk_1^- x_f} & -M_2^+ \frac{c_1}{c_2} e^{jk_2^+ x_f} & M_2^- \frac{c_1}{c_2} e^{-jk_2^- x_f} & M_2 \frac{c_1}{c_2} \\ M_1^{+2} e^{jk_1^+ x_f} & -M_1^{-2} e^{-jk_1^- x_f} & -M_2^{+2} e^{jk_2^+ x_f} & M_2^{-2} e^{-jk_2^- x_f} & M_2^2 \\ \mathcal{M}_{31} & \mathcal{M}_{32} & \mathcal{M}_{33} & \mathcal{M}_{34} & \frac{M_2^3}{2} \\ M_1^+ & -M_1^- & 0 & 0 & 0 \\ 0 & 0 & \mathcal{T}_m e^{jk_2^+ L} & -\mathcal{T}_p e^{-jk_2^- L} & -\frac{M_2}{2} e^{jk_s(L-x_f)} \end{bmatrix} \tag{42}$$

$$\mathcal{M}_{31} = \frac{c_1}{c_2}\left(M_1^+\left[M_1 + 1/(\gamma-1) + M_1^2/2\right]\right)e^{jk_1^+ x_f}$$

$$\mathcal{M}_{32} = \frac{c_1}{c_2}\left(M_1^-\left[M_1 - 1/(\gamma-1) - M_1^2/2\right]\right)e^{-jk_1^- x_f}$$

$$\mathcal{M}_{33} = -\left(M_2^+\left[M_2 + 1/(\gamma-1) + M_2^2/2\right]\right)e^{jk_2^+ x_f}$$

$$\mathcal{M}_{34} = -\left(M_2^-\left[M_2 - 1/(\gamma-1) - M_2^2/2\right]\right)e^{-jk_2^- x_f}$$

with $M_1^+ = (1+M_1)$, $M_1^- = (1-M_1)$, $M_2^+ = (1+M_2)$, $M_2^- = (1-M_2)$, $\mathcal{T}_m = (1-((\gamma-1)/2)M_2)$ and $\mathcal{T}_p = (1+((\gamma-1)/2)M_2)$.

4.3 Method B2: Delayed Entropy Coupled Boundary Condition Approach. Combining Eqs. (11), (38), and (40), and taking the limit $u \to 0$ while the product $u_2\hat{s}$ remains finite [2], one obtains the following expression for the entropy produced by the flame:

$$\hat{s}_2(x_f) = -\frac{C_p^2(T_{02}-T_{01})(\gamma-1)}{u_2 c_2^2}\frac{\rho_1}{\rho_2}\hat{u}_1(x_f) \tag{43}$$

Entropy fluctuations at the exit $x = L$ may be analytically expressed by the addition of a time delay that mimics the mean flow convective effect,

$$\hat{s}_2(L) = \hat{s}_2(x_f)e^{j\omega\tau_s} \quad \text{with } \tau_s = \frac{L-x_f}{u_2} \tag{44}$$

The methodology explained in the previous section is applied to Eq. (41), by reformulating this boundary condition thanks to an energetical and isentropic functional $f(\hat{J}, \hat{m}, \hat{s}) = 0$. It becomes

$$\hat{m}\left(\frac{c_2 + 1/2(\gamma-1)M_2u_2}{(1-M_2^2)}\right) - \hat{J}\left(\frac{\rho_2 M_2 + 1/2(\gamma-1)M_2\rho_2}{(1-M_2^2)}\right) - \frac{1}{2}M_2\rho_2 c_2^2\frac{\hat{s}_2}{C_p} = 0$$

Reformulating this equation by using waves and injecting the limiting behaviors Eq. (29) leads to

$$\frac{A^+}{1+M_2}\left(1 - \frac{1}{2}(\gamma-1)M_2\right) - \frac{A^-}{1-M_2}\left(1 + \frac{1}{2}(\gamma-1)M_2\right) = 0 \tag{45}$$

This condition handles properly the acoustic reflection that arises when a nozzle is connected to a domain computed under the zero Mach number assumption. However, it does not represent the entropy/acoustic coupling since σ was set to zero in agreement with Eq. (29). This is the objective of the DECBC approach to model the effect of the accelerated entropy fluctuations on the acoustics within the zero Mach number region. To this purpose, the modeled entropy at the domain exit, Eq. (44), is injected into Eq. (45) while keeping the energetical form given by the functional at Eq. (45). Expressing $\hat{u}_1(x_f)$ in terms of waves A_1^+ and A_1^- allows us to write the following condition at $x = L$:

$$A_1^+\left[\beta e^{jk_1 x_f}\right] - A_1^-\left[\beta e^{-jk_1 x_f}\right] + A_2^+\left[\frac{(1-\frac{\gamma-1}{2}M_2)e^{jk_2 L}}{1+M_2}\right] - A_2^-\left[\frac{(1+\frac{\gamma-1}{2}M_2)e^{-jk_2 L}}{1-M_2}\right] = 0 \tag{46}$$

with

$$\beta = \frac{1}{2}C_p\frac{(T_2-T_1)(\gamma-1)}{c_1 c_2}e^{j\omega\tau_s} \tag{47}$$

As in the previous section, the proper inlet boundary condition leads to $A_1^+ - A_1^- = 0$. Finally, the problem defined by the matrix of Eq. (42) reduces to Eq. (48),

$$\begin{bmatrix} \frac{e^{jk_1 x_f}}{\rho_1 c_1} & -\frac{e^{-jk_1 x_f}}{\rho_1 c_1} & -\frac{e^{jk_2 x_f}}{\rho_2 c_2} & \frac{e^{-jk_2 x_f}}{\rho_2 c_2} \\ e^{jk_1 x_f} & -e^{-jk_1 x_f} & -e^{jk_2 x_f} & -e^{-jk_2 x_f} \\ 1 & -1 & 0 & 0 \\ \beta e^{jk_1 x_f} & -\beta e^{-jk_1 x_f} & \frac{(1-\frac{\gamma-1}{2}M_2)e^{jk_2 L}}{1+M_2} & -\frac{(1+\frac{\gamma-1}{2}M_2)e^{-jk_2 L}}{1-M_2} \end{bmatrix} \tag{48}$$

Consistently with the no flow approximation, Mach numbers M_1 and M_2 do not appear in the first two rows which describe the wave propagation within the cold and burnt gases.

4.4 Results. Thermodynamic parameters used in the computation of eigenmodes of the configuration B are presented in Table 3.

Results are presented in Tables 4 and 5. The Mach number M_2 downstream of the flame is a free parameter driving the system,

Table 3 Thermodynamic parameters for configuration *B*

T_1	P_1	T_2	γ	r	L	x_f	x_{th}
300K	101325 Pa	1200 K	1.4	287 SI	1 m	0.5 m	1.087 m

Table 4 Entropic eigenfrequencies computed with methods B0, B1, and B2

M_2	0.0125	0.1
B0	$8.92 - 0.89i$	$67.30 - 5.99i$
B1	$9.36 - 0.80i$	$73.13 - 4.34i$
B2	$8.97 - 0.80i$	$73.65 - 4.11i$

Table 5 Acoustic eigenfrequencies computed with methods B0, B1, and B2. The $*$ symbol refers to respective methods where the coupling with entropy is neglected at the exit boundary condition.

M_2	0.0125	0.1
B0	$206.21 + 25i$	$178.04 + 10.57i$
B1	$211.67 + 5.04i$	$189.02 + 13.7i$
B1 $*$	$211.14 - 2.28i$	$210.76 - 18.51i$
B2	$211.67 + 5.34i$	$192.27 + 18.63$
B2 $*$	$211.14 - 0.82i$	$210.66 - 6.6i$

which is computed directly by the equations with methods **B0** and **B1**, and prescribed in the boundary condition formulation with method **B2**. The behavior of the real part of the first eigenfrequency computed with methods **B0**, **B1**, and **B2** show a strong dependency on the mean flow Mach number. The real part of the frequency is proportional to the convective time delay of the flow, suggesting that this eigenmode is of entropic nature. The second eigenmode computed does not present the same behavior and the real part of the frequency is approximately the same whichever the method used or the Mach number prescribed. As shown in Sec. 3, the influence of increasing the mean flow velocity is to damp the imaginary part, suggesting the presence of an acoustic eigenmode.

A good agreement is found between analytical methods **B1** and **B2** and the numerical reference method **B0**, except that this last one mispredicts the imaginary part of the eigenmodes and underpredicts the real part of acoustic eigenfrequencies. Such discrepancies can be explained by the fact that method B0 solves the whole domain (the combustor plus the nozzle), while methods **B1** and **B2** are limited by the low-frequency compact model which does not take into account the length of the nozzle or the phase shift between incoming and reflected waves [24]. However, such a simplified model shows at the first order that the use of a DECBC is able to capture both entropic and acoustic eigenmodes and to predict them correctly, despite the fact that the mean flow is neglected during the computation of the domain. In order to illustrate the effect of the coupling with entropy, methods **B1*** and **B2*** present the computation of eigenmodes with a purely acoustic boundary condition, i.e., the coupling with entropy waves has been neglected in Eq. (41) (this means using Eq. (45) instead of Eq. (46)). Obviously the entropic mode does not appear in this case. The growth rate of the acoustic mode is significantly mispredicted, suggesting that the coupling between entropy and acoustic fluctuations exhibit a strong unstable thermoacoustic mode, while purely acoustic analysis shows a stable eigenmode.

5 Conclusions

The present study is devoted to the modeling of mean flow effect while computing thermoacoustic eigenmodes under the zero Mach number assumption. It has been shown that

- When the computational domain is represented under the no flow assumption, the acoustic impedance modeling a compressor or a turbine must be prescribed under an energetical form rather than from the classical acoustic variables. A systematic methodology is proposed to generate the proper reflection coefficient to impose given any physical boundary condition written without the zero Mach number assumption.
- The coupling between entropy and acoustic waves at the entrance of a nozzle generates a low frequency eigenmode and a shift of higher frequency modes that does not appear when the mean flow convective effects are neglected. Such phenomena can be taken into account thanks to the proposed methodology where a zero Mach number formulation is used together with a delayed entropy coupled boundary condition.

Nomenclature

A^+, A^- = amplitudes of forward and backward acoustic waves
Cp = heat capacity per mass unit at fixed pressure
Cv = heat capacity per mass unit at fixed volume
J = total enthalpy
M = Mach number
R = reflection coefficient
Z = complex impedance
c = sound celerity
k = wave number
m = mass flow rate
p = static pressure
q = heat release per unit volume
s = entropy per mass unit
u = velocity vector
ρ = density
$\hat{g}$ = complex amplitude of the fluctuating quantity g
DECBC = delayed entropy coupled boundary condition

References

[1] Lieuwen, T., and Yang, V., 2005, "Combustion Instabilities in Gas Turbine Engines. Operational Experience, Fundamental Mechanisms and Modeling," *Progress in Astronautics and Aeronautics*, Vol. 210, AIAA, Reston, VA.
[2] Dowling, A. P., 1995, "The Calculation of Thermoacoustic Oscillations," J. Sound Vib., **180**(4), pp. 557–581.
[3] Polifke, W., Poncet, A., Paschereit, C. O., and Doebbeling, K., 2001. "Reconstruction of Acoustic Transfer Matrices by Stationary Computational Fluid Dynamics," J. Sound Vib., **245**(3), pp. 483–510.
[4] Selle, L., Benoit, L., Poinsot, T., Nicoud, F., and Krebs, W., 2006, "Joint Use of Compressible Large-Eddy Simulation and Helmoltz Solvers for the Analysis of Rotating Modes in an Industrial Swirled Burner," Combust. Flame, **145**(1–2), pp. 194–205.
[5] Lieuwen, T., 2003, "Modeling Premixed Combustion-Acoustic Wave Interactions: A Review," J. Propul. Power, **19**(5), pp. 765–781.
[6] Morfey, C. L., 1973, "Amplification of Aerodynamic Noise by Convected Flow Inhomogeneities," J. Sound Vib., **31**, pp. 391–397.
[7] Williams, J. E. F., and Howe, M. S., 1975, "The Generation of Sound by Density Inhomogeneities in Low Mach Number Nozzle Flows," J. Fluid Mech., **70**(03), pp. 605–622.
[8] Howe, M., 1975, "Contributions to the Theory of Aerodynamic Sound, With Application to Excess Jet Noise and the Theory of the Flute," J. Fluid Mech., **71**(04), pp. 625–673.
[9] Candel, S., 1975. "Acoustic Conservation Principles, Application to Plane and Modal Propagation in Nozzles and Diffusers," J. Sound Vib., **41**, pp. 207–232.
[10] Polifke, W., Paschereit, C. O., and Döbbeling, K., 2001, "Constructive and Destructive Interference of Acoustic and Entropy Waves in a Premixed Combustor With a Choked Exit," Int. J. Acoust. Vib., **6**(3), pp. 135–146.
[11] Bloxsidge, G., Dowling, A., Hooper, N., and Langhorne, P., 1988, "Active Control of Reheat Buzz," AIAA J., **26**, pp. 783–790.
[12] Nicoud, F., and Wieczorek, K., 2009, "About the Zero Mach Number Assumption in the Calculation of Thermoacoustic Instabilities," Int. J. Spray Combust. Dyn., **1**, pp. 67–112.

[13] Rao, P., and Morris, P., 2006, "Use of Finite Element Methods in Frequency Domain Aeroacoustics," AIAA J., **44**, pp. 1643–1652.
[14] Davies, P. O. A. L., 1988, "Practical Flow Duct Acoustics," J. Sound Vib., **124**(1), pp. 91–115.
[15] Sattelmayer, T., 2003, "Influence of the Combustor Aerodynamics on Combustion Instabilities From Equivalence Ratio Fluctuations," J. Eng. Gas Turbine Power, **125**, pp. 11–19.
[16] Marble, F. E., and Candel, S., 1977, "Acoustic Disturbances From Gas Nonuniformities Convected Through a Nozzle," J. Sound Vib., **55**, pp. 225–243.
[17] Lamarque, N., and Poinsot, T., 2008, "Boundary Conditions for Acoustic Eigenmodes Computation in Gas Turbine Combustion Chambers," AIAA J., **46**(9), pp. 2282–2292.
[18] Peters, M., Hirschberg, A., Reijnen, A., and Wijnands, A., 1993, "Damping and Reflection Coefficient Measurements for an Open Pipe at Low Mach and Low Helmholtz Numbers," J. Fluid Mech., **256**, pp. 499–499.
[19] Cantrell, R., and Hart, R., 1964, "Interaction Between Sound and Flow in Acoustic Cavities: Mass, Momentum, and Energy Considerations," J. Acoust. Soc., **36**, p. 697.
[20] Doak, P., 1998, "Fluctuating Total Enthalpy as the Basic Generalized Acoustic Field," Theor. Comput. Fluid Dyn., **10**(1), pp. 115–133.
[21] Leyko, M., Moreau, S., Nicoud, F., and Poinsot, T., 2011, "Numerical and Analytical Modelling of Entropy Noise in a Supersonic Nozzle With a Shock," J. Sound Vib., **330**(16, 1), pp. 3944–3958.
[22] Hield, P., Brear, M., and Jin, S., 2009, "Thermoacoustic Limit Cycles in a Premixed Laboratory Combustor With Open and Choked Exits," Combust. Flame, **156**(9), pp. 1683–1697.
[23] Macquisten, M. A., and Dowling, A. P., 1994, "Low-Frequency Combustion Oscillations in a Model Afterburner," Combust. Flame, **94**(4), pp. 253–264.
[24] Goh, C., and Morgans, A., 2011, "Phase Prediction of the Response of Choked Nozzles to Entropy and Acoustic Disturbances," J. Sound Vib., **330**(21), pp. 5184–5198.